



**HAL**  
open science

# Theoretical approach to point defects in a single transition metal dichalcogenide monolayer: conductance and force calculations in MoS<sub>2</sub>

César González, Yannick J Dappe

► **To cite this version:**

César González, Yannick J Dappe. Theoretical approach to point defects in a single transition metal dichalcogenide monolayer: conductance and force calculations in MoS<sub>2</sub>. *Comptes Rendus. Physique*, 2021, 22 (S4), pp.1-19. 10.5802/crphys.72 . hal-03315743

**HAL Id: hal-03315743**

**<https://hal.science/hal-03315743>**

Submitted on 5 Aug 2021

**HAL** is a multi-disciplinary open access archive for the deposit and dissemination of scientific research documents, whether they are published or not. The documents may come from teaching and research institutions in France or abroad, or from public or private research centers.

L'archive ouverte pluridisciplinaire **HAL**, est destinée au dépôt et à la diffusion de documents scientifiques de niveau recherche, publiés ou non, émanant des établissements d'enseignement et de recherche français ou étrangers, des laboratoires publics ou privés.



INSTITUT DE FRANCE  
Académie des sciences

# *Comptes Rendus*

---

## *Physique*

César González and Yannick J. Dappe

**Theoretical approach to point defects in a single transition metal dichalcogenide monolayer: conductance and force calculations in MoS<sub>2</sub>**


Online first, 25th May 2021

<<https://doi.org/10.5802/crphys.72>>

**Part of the Special Issue:** Recent advances in 2D material physics

**Guest editors:** Xavier Marie (INSA Toulouse, Université Toulouse III Paul Sabatier, CNRS, France) and Johann Coraux (Institut Néel, Université Claude Bernard Lyon 1, France)

© Académie des sciences, Paris and the authors, 2021.  
*Some rights reserved.*

 This article is licensed under the  
CREATIVE COMMONS ATTRIBUTION 4.0 INTERNATIONAL LICENSE.  
<http://creativecommons.org/licenses/by/4.0/>



*Les Comptes Rendus. Physique sont membres du  
Centre Mersenne pour l'édition scientifique ouverte*  
[www.centre-mersenne.org](http://www.centre-mersenne.org)



---

Recent advances in 2D material physics / *Physique du solide 2D*

# Theoretical approach to point defects in a single transition metal dichalcogenide monolayer: conductance and force calculations in MoS<sub>2</sub>

*Approche théorique pour les défauts ponctuels dans une monocouche de dichalcogénure de métal de transition : calculs de conductance et de force dans le MoS<sub>2</sub>*

César González\*,<sup>ⓐ</sup> <sup>ⓑ</sup> *a, b* and Yannick J. Dappe\*,<sup>ⓐ</sup> <sup>ⓒ</sup> *c*

<sup>a</sup> Departamento de Física de Materiales, Universidad Complutense de Madrid, E-28040 Madrid, Spain

<sup>b</sup> Instituto de Magnetismo Aplicado UCM-ADIE, Vía de Servicio A-6, 900, E-28232 Las Rozas de Madrid, Spain

<sup>c</sup> SPEC, CEA, CNRS, Université Paris-Saclay, CEA Saclay, 91191 Gif-sur-Yvette Cedex, France

*E-mails:* cesar.gonzalez@ucm.es (C. González), yannick.dappe@cea.fr (Y. J. Dappe)

**Abstract.** We present here a small review on our exhaustive theoretical study of point defects in a MoS<sub>2</sub> monolayer. Using Density Functional Theory (DFT), we characterize structurally and electronically different kinds of defects based on S and Mo vacancies, as well as their antisites. In combination with a Keldysh–Green formalism, we model the corresponding Scanning Tunneling Microscopy (STM) images. Also, we determine the forces to be compared with Atomic Force Microscopy (AFM) measurements, and explore the possibilities of molecular adsorption. Our method, as a support to experimental measurements allows to clearly discriminate the different types of defects. Finally, we present very recent results on lateral conductance calculations of defective MoS<sub>2</sub> nanoribbons. All these findings pave the way to novel applications in nanoelectronics or gas sensors, and show the need to further explore these new systems.

**Résumé.** Nous présentons ici une mini-revue de nos différents travaux sur l'étude théorique des défauts dans une monocouche de MoS<sub>2</sub>. En utilisant la Théorie de la Fonctionnelle de la Densité (DFT), nous avons caractérisé structurellement et électroniquement différents types de défauts à partir de lacunes de S et Mo, ainsi que leurs antisites. En combinaison avec un formalisme de Green–Keldysh, nous avons simulé les images de microscopie à effet tunnel (STM) correspondantes. Egalement, nous avons déterminé les forces,

---

\* Corresponding authors.

afin d'interpréter les expériences de microscopie à force atomique (AFM). Nous avons également étudié l'adsorption de molécules sur ces défauts. Finalement, nous présentons de récents résultats sur le calcul de conductance latérale dans des nano-rubans de MoS<sub>2</sub> avec défauts. Ces travaux ouvrent la voie à de nouvelles applications en nanoélectronique ou pour les capteurs de gaz, et soulignent la nécessité d'explorer plus avant ces nouveaux systèmes.

**Keywords.** Electronic structure, Defects, MoS<sub>2</sub>, DFT, STM/AFM, Molecular adsorption.

**Mots-clés.** Structure électronique, Défauts, MoS<sub>2</sub>, DFT, STM/AFM, Adsorption moléculaire.

Online first, 25th May 2021

## 1. Introduction

The rise of graphene and, in particular, the possibility of isolating one atomic layer from graphite, has participated to an important revolution in nanoelectronics [1]. Indeed, graphene is well-known now as a bidimensional material with fascinating electronic properties like high conductivity or massless Dirac fermions [2–4]. But in a second time, the discovery of graphene has also shed light on a whole world of new bidimensional materials. For example, hexagonal boron nitride (hBN) as the graphene counterpart made of boron and nitrogen is widely used due to its widegap and its encapsulation properties [5, 6]. Also we have seen the emergence of the great family of transition metal dichalcogenides (TMDC), made of a transition metal layer sandwiched in between two chalcogen atom layers, and presenting several different properties [7–10]. Among the most common ones, we can consider metallic or semiconductor behaviors, superconductors, ferromagnets, etc... in other words, the full Solid State Physics can be found in these 2D materials [11]. As such, these new materials open a wide spectrum of exciting perspectives for the development of nanoelectronics. For example, besides electronic properties, these materials present interesting thermal conductivity in the plane and at the interface between two layers, with important applications for thermoelectronic devices [12]. A dedicated theoretical study has revealed the important role of phonon scattering at the interface between the layers [13].

Another important aspect lies in the fact that these materials can be combined to form new nano-architectures presenting different properties. Hence, exploiting the weak and van der Waals (vdW) interactions between these atomic layers, one can assemble different 2D materials and take advantage of the different properties to create new multielectronic devices [14]. These assemblies are called van der Waals heterostructures, and constitute a very active field of research nowadays [15, 16]. Very recently, researchers have even developed new types of van der Waals heterostructures, namely 1D van der Waals heterostructures [17].

When considering electronic properties in whichever material, one cannot avoid the question of defects. Indeed, fabrication of materials implies necessarily the creation of defects. Even more relevant when growing 2D materials, it is clear that we will observe the creation of vacancies, atomic substitutions or atomic or molecular impurities adsorbed on the surface of the material [18–20]. Considering the low electronic density of such materials, such defects will obviously affect their electronic properties, for example by inducing metallic states or modifying the original electronic gap of the material. As a consequence, electronic transport properties or chemical reactivity might be modified [21, 22]. On another hand, one can think about exploiting these new induced properties to create new nanoelectronic devices. Indeed, starting from a well-known electronic material and modifying its atomic structure by creating controlled defects allows to shape its electronic properties in a desired direction. In that respect, a major challenge nowadays to control the creation of such defects is also an accurate characterization at the

atomic level [19, 20, 23]. Such a characterization can rely on atomic probe microscopies such as Scanning Tunneling Microscopy (STM) or Atomic Force microscopy (AFM) which allow us to characterize the local electronic density or the local atomic forces. Indeed, conductance or force measurements are very useful to determine a local chemical environment and its subsequent incidence on the electronic properties [24–26]. However, these techniques are rather complex to interpret and the help of theory and modelling is often welcome to ensure a good understanding of the acquired results. For example, Density Functional Theory (DFT) calculations allow a modelling at the atomic level with a high accuracy on the electronic properties, providing an excellent support to experimental results [27, 28].

To illustrate this approach, we present here a mini-review of our recent results on atomic defect simulations in 2D materials. We consider here the well-known molybdenum disulfide ( $\text{MoS}_2$ ), which is a 2D semiconductor presenting the peculiar characteristic of having a direct gap in the monolayer phase, and an indirect gap for thicker films. This material originally used as a lubricant for engines since decades is very promising for nanoelectronics and optoelectronics applications [29–31]. Also, besides some Scanning Transmission Electronic Microscopy (STEM) or STM experiments, rather few studies of atomic or substitutional defects have been performed on this material [19, 20]. In particular, on a theoretical point of view, an exhaustive study of defects in  $\text{MoS}_2$  was clearly missing.

The organization of the article is the following: in the next section, we will present the main results obtained on the modelling of atomic and substitutional defects in  $\text{MoS}_2$ . Starting from the pristine  $\text{MoS}_2$ , we will consider the main possible defects like Mo or S vacancies, and we will address them by STM images modelling, through electronic conductance calculations, and AFM modelling through force calculations. In Section 3, we will consider these defects under the angle of molecular adsorption, in particular to check the reactivity of the defects and to determine how the molecules affect the electronic properties. Section 4 will be devoted to new calculations on lateral  $\text{MoS}_2$  junctions: we consider a defective  $\text{MoS}_2$  nanoribbon sandwiched between gold electrodes and we determine the corresponding conductance, to be compared with the vertical conductance discussed in Section 2. Finally, we conclude and bring some perspectives on this general topic.

## 2. Point defects in a $\text{MoS}_2$ monolayer

In this section, we will consider the main potential point defects in a layer of  $\text{MoS}_2$  through STM and AFM modelling. First, we start with pristine  $\text{MoS}_2$ , in order to present the general characteristics of this system and to present briefly the computational method used here.

### 2.1. *Pristine $\text{MoS}_2$*

For all the calculations presented here, described in full details in Ref. [32], we have considered a  $6 \times 4$  rectangular unit cell of  $\text{MoS}_2$  (72 atoms), as represented in Figure 1(a). Calculations including structural relaxations and electronic structure determination have been performed using the very efficient DFT localised-orbital molecular dynamics package FIREBALL [33–35]. This code is based on a self-consistent version of the Harris–Foulkes functional, which allows to perform the self-consistency over the occupation numbers [36, 37]. Also, the exchange correlation energy is calculated according to the multi-centre weighted approximation (McWEDA, which corresponds to an LDA formalism in the Harris–Foulkes functional) [34]. Finally, FIREBALL uses a localized optimised basis set [38] and we have used cutoff radii (in atomic units) of  $s = 3.1$  and  $6.2$ , and  $p = 3.9$  and  $6.2$  for S and Mo respectively, and  $d = 5.8$  for Mo.

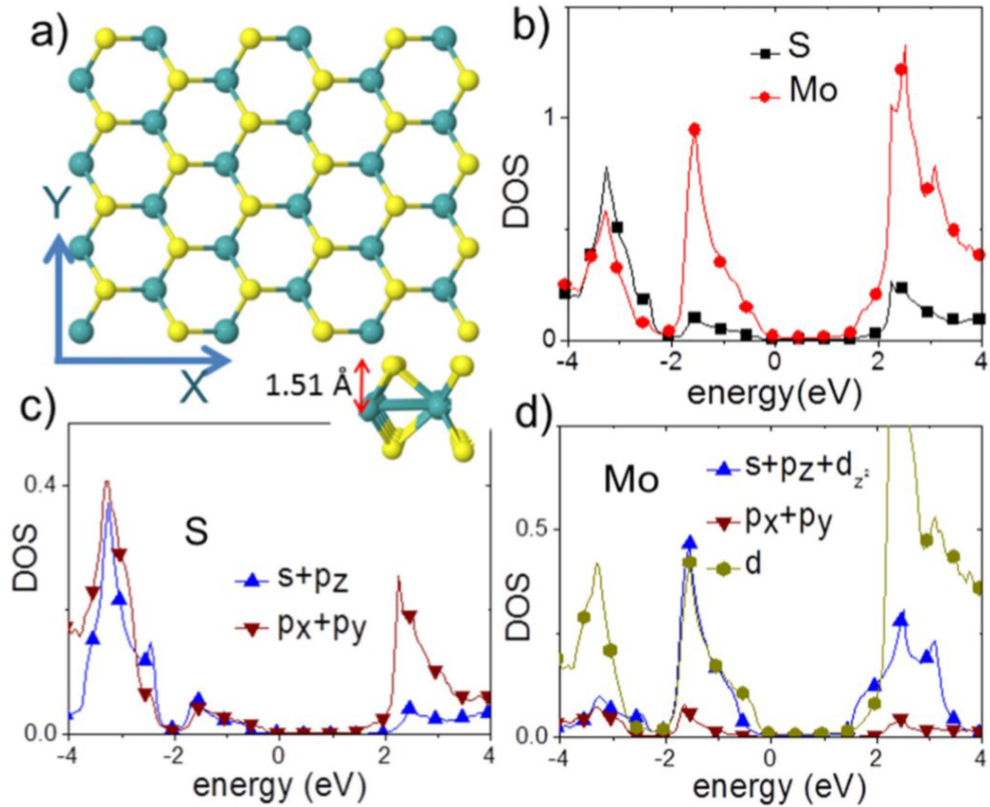


**Figure 1.** (a) Top and side view of the atomic structure of a clean single layer of MoS<sub>2</sub> (yellow/blue spheres are S/Mo). The arrows indicate the X and Y directions of the lattice vectors used in the calculation. (b) Calculated electronic DOS for S (black squares) and Mo (red circles) atoms; (c) and (d) show the orbital contributions to the atomic DOS of the S and Mo atoms, respectively. The DOS are separated into directional  $s + p_z + d_z^2$  orbitals (blue up-triangles), in-plane  $p_x + p_y$  (down-triangles) and the sum of the other four d orbitals (yellow hexagons). Reprinted with permission from Ref. [32], copyright IOP 2016.

First, we have optimized the geometry of the pristine MoS<sub>2</sub> using the  $6 \times 4$  unit cell, until the forces have reached a value lower than  $0.05 \text{ eV}/\text{\AA}$ . From this optimized geometry, we have calculated the Density of States (DOS) of the system, and its different contributions from the different Mo and S orbitals, as represented in Figure 1(b–d). As a result, we can observe an electronic gap around  $1.7 \text{ eV}$ , mostly dominated by the electronic contribution of Mo. Taking a closer look at the different orbital contributions, we can deduce that the valence band is mostly dominated by Mo  $s + p_z + d_z^2$  orbitals, and in a minor amplitude, other Mo  $d$  states. Also, the conduction band is dominated by the other  $d$  orbitals of Mo. On another hand, S atoms contribute to the valence and conduction bands mainly through their  $p_x + p_y$  states.

From this electronic structure, adding an atomic tip to the system to mimic the STM experiment, for example a 35-gold atoms pyramid [32], we can now simulate the corresponding STM image of the pristine MoS<sub>2</sub>, in order to set a reference to compare with defect calculations or further experimental results. To this end, the STM current is calculated based on the Keldysh–Green formalism, which uses the DOS of the STM tip ( $\rho_{TT}$ ), the DOS of the system ( $\rho_{SS}$ ) considered (MoS<sub>2</sub> here), and the tip-sample interaction (hoppings  $T_{TS/ST}$ ) extracted from the

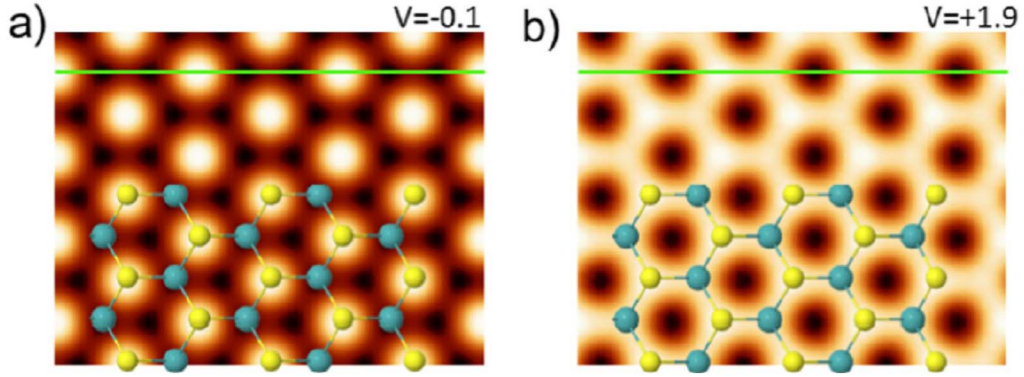


**Figure 2.** Calculated STM images at 4.5 Å and a bias of (a)  $-0.1$  V and (b)  $+1.9$  V for a clean MoS<sub>2</sub> monolayer. The STM images were graphed using WSxM software [40]. Reprinted with permission from [32], copyright IOP 2016.

Fireball calculations. In that respect, the calculated current at 0 K temperature is expressed as:

$$I = \frac{4\pi e^2}{h} \int_{E_F}^{E_F+eV} \text{Tr}[T_{TS}\rho_{SS}(\omega)D_{SS}^r(\omega)T_{ST}\rho_{TT}(\omega-eV)D_{TT}^a(\omega-eV)]d\omega, \quad (1)$$

where  $D_{TT}^a$  and  $D_{SS}^r$  are complex matrices corresponding to multiple scattering effect produced by the possible electronic reflections occurring when the tip is close to the sample. Of course, at standard STM distances, these matrices are equal to identity and disappear from the formula. Finally, a full description of the methodology can be found in [39]. As a result, we present in Figure 2 the calculated STM images for pristine MoS<sub>2</sub> at (a) negative voltages, probing occupied states, and (b) positive voltages, probing unoccupied states.

The main important feature, is that at negative voltage, we only observe sulfur atoms, meanwhile at positive voltages, we can observe sulfur and molybdenum atoms. This is due to the effect of the STM tip-atom distance combined with the DOS contributions calculated previously. Indeed, at negative voltages, both S and Mo DOS are equivalent, but the tip-Mo distance is larger than the tip-S, which favors the emergence of the S DOS in the STM image. Oppositely, at positive voltages, we have the same distance ratio, but the DOS of Mo is much larger than the one of S, which compensates the distance and makes the two types of atoms contribute to the STM images. This result can be understood in terms of the electronic hopping ( $T_{ST}$  and  $T_{TS}$  matrices in (1)). It measures the probability of an electron to jump between the tip and the sample. These values decrease exponentially with the distance, reducing drastically the contribution of the atoms at lower positions even though they can present much larger DOS. Consequently, we can deduce that the STM image gives us information not only on the respective DOS of the probed atoms, but also on their respective positions, even at different heights.

In the next subsection, we will see how we can use STM to characterize the main types of point defects in MoS<sub>2</sub>.

## 2.2. Defective MoS<sub>2</sub>: Scanning Tunneling Microscopy and conductances

The main point defects that we have considered here are related to Mo and S vacancies, and their respective antisites through atomic substitutions [32]. Namely, we consider Mo vacancy, S vacancy, S divacancy, and the corresponding substitutions like one or two S in a Mo vacancy, a Mo in a S vacancy, and one or two Mo in a S divacancy. These defects are very common in MoS<sub>2</sub>

**Table 1.** Formation energy in eV of the different defects on the MoS<sub>2</sub> monolayer: S vacancy (vS), Mo vacancy (vMo), S divacancy (v2S), one or two S atoms occupying the Mo vacancy (vMo+S and vMo+S2) and one or two Mo atoms in a S mono- and divacancy (vS+Mo, v2S+Mo and v2S+Mo2, respectively)

|            | vS   | v2S  | vMo  | vS+Mo | v2S+Mo | v2S+Mo2 | vMo+S | vMo+S2 |
|------------|------|------|------|-------|--------|---------|-------|--------|
| $E_f$ (eV) | 2.57 | 5.14 | 7.22 | 5.55  | 7.42   | 10.75   | 6.35  | 9.04   |

The formation energies have been calculated using the energy in a perfect Mo or S bulk. Reprinted with permission from Ref. [46], copyright RSC 2017.

growth and can also be controlled in a rather easy manner by removing atoms. For a monolayer formed by  $N_{\text{Mo}}$  and  $N_{\text{S}}$  atoms, the formation energy can be expressed as [41]:

$$E_f = E_t - N_{\text{Mo}}E(\text{Mo}) - N_{\text{S}}E(\text{S}) \quad (2)$$

$E(\text{Mo})$  and  $E(\text{S})$  are the atomic energies of a single Mo or S atom respectively, in a perfect Mo or S bulk, and  $E_t$  is the total energy of the system. These formation energies have been calculated using the DFT-plane wave Vienna *Ab initio* Simulation Package VASP code [42–44], based on the pseudopotential approximation following the projector augmented wave (PAW) approach. More technical details about the calculations can be found in Ref. [45]. The corresponding results are presented in Table 1.

From these results, we can observe that the S vacancy presents the lowest formation energy (2.57 eV), which makes it very favorable to appear during the MoS<sub>2</sub> growth process, in good agreement with experiments [20]. Also, the formation energy of the S divacancy is twice the one of the S vacancy, meaning that it is the same cost to remove two S atoms independently. Comparatively, the creation of one Mo vacancy presents a formation energy of 7.22 eV, much higher, which is representative of the strong Mo–Mo bonding in MoS<sub>2</sub>. Overall, a general trend lies in the stability of these defects, which has also been probed using Molecular Dynamics simulations [46], and which makes them promising system to consider for nanoelectronics applications.

The corresponding calculated STM images are represented in Figure 3. Looking at the images, a first point we can stress is that the global MoS<sub>2</sub> network is not drastically affected by the Mo or S vacancies. Indeed, apart when substituting the atoms, we observe more dangling bonds, with brilliant density trace in the STM image, than real surface reconstruction. For example, we can observe brilliant traces in the neighborhood of the missing atoms in Figure 3(a), (d) and (f), corresponding respectively to Mo, S and two S vacancies. As a consequence, we can expect from these dangling bonds an important local reactivity, making these sites very favorable for molecular adsorption, as we will see in the next section. Also, these changes in the local electronic density are obviously reflected in the electronic gap. Hence, in all the cases considered here, the gap is reduced from the pristine MoS<sub>2</sub> gap of 1.7 eV, to 1.0 eV in the S vacancy structure, 0.8 eV in the S divacancy, around 0.6 eV in the Mo and S substituted Mo vacancy, and no more gap for the other structures. This is attributed to the emergence of new states in the original gap, namely dangling bonds in vacancy configurations, or extra localized states in atomic substitutions. In particular, in the cases where the gap fully disappears, the substitution of S atoms in the S mono- or divacancies by Mo atoms induces new metallic states that fill the electronic gap. These states are mainly of  $d_z^2$  character, originating of course from the substituting Mo atoms. They can be observed in the calculated DOS of Ref. [32] and can be attributed to the non-passivation of the substituting Mo atoms. It has to be noted that two S substitutions in a Mo vacancy yields a half-occupied state at the Fermi level, and a gap of 1.25 eV from this state until the first unoccupied state. Regarding S substitutions in Mo vacancies, it is important to stress that the new structure



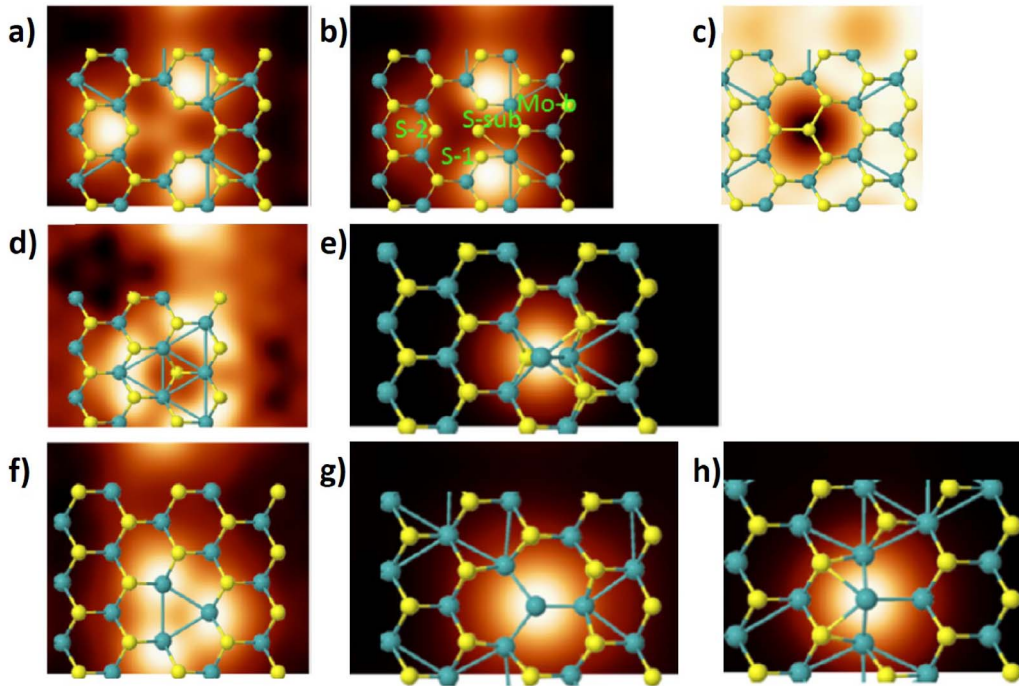


**Figure 3.** Calculated STM images at 4.5 Å and a bias of +1.9 V for (a) a Mo vacancy, (b) a Mo vacancy with a substitutional S atom, (c) a Mo vacancy with two substitutional S atoms, (d) a S vacancy, (e) a S vacancy with a substitutional Mo atom, (f) a S divacancy, (g) a S divacancy with a Mo substitutional atom and (h) a S divacancy with two Mo substitutional atoms in a MoS<sub>2</sub> monolayer. The corresponding atomic configurations are superimposed (yellow/blue spheres represent S/Mo atoms). The STM images were graphed using the WSxM software [40]. Reprinted with permission from Ref. [32], copyright IOP 2016.

tries to mimic the original MoS<sub>2</sub> structure, which sets the S atoms in the plane. Therefore, there is no additional corrugation in the system by substituting S atoms to the original Mo atoms. The main difference between S mono- and divacancy lies in the reactivity of the site, the removing of a second S atom leading obviously to more dangling bonds. In addition, the substitution of 2 S atoms by two Mo atoms leads also to a more metallic site.

This study reveals that the STM images of defective MoS<sub>2</sub> are strongly affected by the geometry of the system, even though the MoS<sub>2</sub> network surrounding the defect remains globally unaffected. Hence, the removal of Mo or S atoms induces protrusions associated to dangling bonds while the substitution of these atoms add metallic states and reduce the gap. The method developed here is anyway very powerful, as the images at different biases can be analyzed, in conjunction with the calculated DOS, in quest for specific peaks which constitute the fingerprint of the considered defect. Hence, this tool complements the experimental measurements, and it has been used as such for example in the discrimination of a nitrogen atom substitution in a S vacancy in a MoS<sub>2</sub> layer probed by STM [47]. Obviously, more complex defects like grain boundaries [48, 49] or molecular adsorption as we will discuss in the next section, can also be characterized using the same method. Finally, this study also reveals the potential ability of defects in MoS<sub>2</sub> for future nanoelectronics, through the local semiconductor/metal transition, or gas sensors upon molecular adsorption, which both affect the local DOS, and that can be detected

through electronic conductance measurements. To illustrate this perspective, in the last section of this article, we propose a model of lateral MoS<sub>2</sub> junction sandwiched between two gold electrodes, where the electronic conductance of the system is measured and varies as a function of the considered defect.

In the next subsection, we will consider another type of local probe spectroscopy, namely force measurements through AFM, to further characterize defects in MoS<sub>2</sub>.

### 2.3. Defective MoS<sub>2</sub>: Atomic Force Microscopy and forces

Besides STM measurements which give us access to the local DOS of a system, a complementary spectroscopy lies in AFM experiments, and in particular non-contact AFM, which give us access to the local forces of a system. Obviously forces and local density are related, but the determination of the local forces brings different kind of information on a system. Indeed, we will show here that the defects induce an enhancement of the local reactivity, which is of paramount importance for atomic or molecular adsorption and applications in nanoelectronics.

Here we have considered the same atomic unit cell as for the STM study. However, we have optimized these cells and calculated the forces using VASP [42–44] instead of Fireball. In order to simulate an AFM experiment, we use two type of AFM tips, similarly to the STM tips used for the STM simulations, namely a very reactive Cu one and a much less reactive Si tip. Then the tip has been rigidly approached to the MoS<sub>2</sub> substrate, either pristine or defective, by steps of 0.25 Å, and the system has been fully optimized until the atomic forces reached a value lower than 0.025 eV/Å. The energy curve is then recorded for all the positions, and its derivation leads to the force curves that we use to analyze the different defects here.

The results of force calculations for the different defects and the two types of tips are presented in Figure 4.

As such, Figure 4(a) and (b) represent an atomic picture of the motion of the AFM tip in a Mo vacancy (Cu tip) and S vacancy (Si tip), respectively. This reveals the strong interaction that can occur, leading even to atomic capture. In Figure 4(c–e), we represent the typical force evolution as a function of the tip-surface distance, for different defects in MoS<sub>2</sub>, for the Cu tip, and the same for a Si tip in Figure 4(f–h). In these curves, we look for the minimum, namely the maximal strength of the force (corresponding to the maximal attraction), which is representative of the reactivity of the probed site. Obviously, as the tip approaches the sample, the minimum will be shifted according to the local reactivity of the site, through dangling bonds or local electronic densities, which will change depending on the type of defects and their chemical characteristics. For example, using a Cu tip on the pristine MoS<sub>2</sub>, the difference of force minimum for Mo and S atoms is about 0.7 Å, with very similar forces, i.e.  $-1.00$  nN and  $-0.88$  nN for S and Mo respectively [45]. This difference is explained by the contact difference between the two atoms, since for the S atom we have a direct Cu tip-S atom contact, whereas for the Mo atom, this contact is somehow screened by the neighboring S atoms. Also, we have to bear in mind that the choice of the tip is of high importance to characterize the probed system. Indeed, when determining the interaction forces using a Si tip which is known to be much less reactive, we will obtain this time a higher signal for the Mo atom than for the S atom, due to the establishment of a semiconductor-metal junction that we will discuss later. This explains also why we might obtain different force values with respect to previous results using different kind of AFM tip [50].

Turning to the different defects in MoS<sub>2</sub>, we first consider the result with the Cu tip. We can immediately notice a strong increase in reactivity through the different force minima for the different defect sites. Hence, in Figure 4(c–e), corresponding respectively to the S, Mo and two S vacancies, we have an important force minimum, the most important one corresponding to the Mo vacancy with a deviation of about  $-3.42$  nN. In that respect, this very reactive Mo vacancy

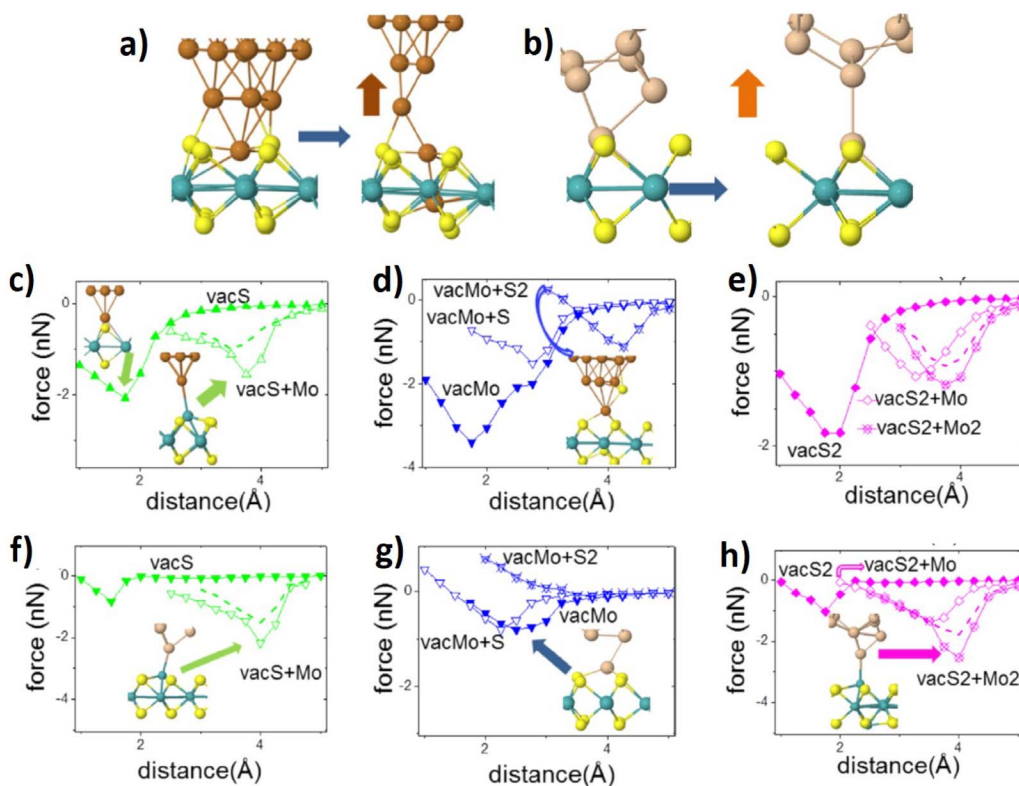


**Figure 4.** Simulation of AFM experiments: two snapshots representing the interaction of (a) a Cu tip with a Mo vacancy and (b) a Si tip with a S vacancy, both with atomic capture. Force curves of a Cu tip interacting with (c) a S and Mo substituted S vacancy, (d) a S mono- and disubstituted Mo vacancy and (e) a Mo mono- and disubstituted S divacancy. In (f–h), same force curves using a Si tip. Reprinted with permission from Ref. [45], copyright ACS 2016.

also presents some exotic effect as the ability of trapping atoms from the tip. This property is illustrated in a snapshot extracted from the simulations in Figure 4(a) where two Cu atoms remain trapped in the Mo vacancy site. This opens the way to specific doping through the use of AFM tip on MoS<sub>2</sub> defects and the creation and control of specific electronic defects. This atomic transfer has been already discussed in other material [51, 52] and is revealed here for 2D materials. Also, what is really interesting is the atomic substitution in MoS<sub>2</sub> vacancies, where a reduction of the reactivity, through the reduction of the forces, is observed. This can be understood through the saturation of the vacancy dangling bonds by the incoming atom for example. Of course the corresponding minima are also shifted due to the specific positions of these new substituting atoms.

A similar analysis can be achieved using a Si tip, which is much more flexible than the Cu tip, and therefore able to explore the defects in an easier manner. Considering the curves presented in Figure 4(f–h), we can observe in general much lower forces compared to the Cu tip, in particular for the interaction with S atoms. This is due to the lower reactivity of the Si tip, as explained before. However, for the defect with Mo substitutional atoms, we recover a strong increase of the tip-atom forces. For example the substitution of two S by two Mo in the S divacancy defect leads to a force of  $-2.55$  nN, twice the value obtained using the Cu tip. We can also observe more

important deformations of the tip, compared to the Cu tip, as a result of the higher flexibility of the Si tip.

In all the cases, we can deduce that the interaction is driven by a standard metal-semiconductor junction. Indeed, the Cu tip is more sensitive to S atoms, whereas the Si tip is more sensitive to the Mo atoms. In both cases, an important charge transfer between the two materials is responsible for the emergence of high forces. In that respect, one has to carefully consider the choice of the AFM tip material in order to carefully image one specific defect or another. Hence, the accurate visualization of a defect fingerprint is closely related to the choice of the AFM tip, either metallic or semiconductor.

In the next section, we will consider the influence of the defect reactivity on the molecular adsorption, and the consequences on their electrical conductance.

### 3. Molecular adsorption on MoS<sub>2</sub> defects and influence on the conductance/force properties

As we have seen in the previous sections, we now know how to discriminate different types of point defects in a MoS<sub>2</sub> layer using different probes like STM or AFM. Moreover, it is possible to have a measure of the local reactivity, through its incidence on the local conductance or on the local forces. In this section, we will consider the adsorption of small molecules on these defects and how they affect the electrical conductance or the local forces. This aspect is very interesting, first in order to probe the reactivity of the defect studied before, but also, in order to design new types of electronic nanodevices, or even gas sensors whose electrical conductance would be affected by the adsorption of a small molecule. This section is divided in two subsections, where we will first consider the adsorption properties, and then their consequences on conductance and forces.

#### 3.1. Molecular adsorption as a probe for local reactivity

We have considered here small inorganic molecules, with size comparable to the size of the point defects considered in this study. Hence, we have performed DFT calculations to characterize the adsorption of CO<sub>2</sub>, CO, H<sub>2</sub>O, NO, NO<sub>2</sub>, H<sub>2</sub> and N<sub>2</sub>, on pristine and defective MoS<sub>2</sub> [46]. The adsorption energy  $E_{\text{Ads}}$  is defined as:

$$E_{\text{Ads}} = E_{\text{tot}} - E_{\text{MoS}_2} - E_{\text{Mol}} \quad (3)$$

where  $E_{\text{tot}}$  is the total energy obtained with VASP for the system containing both the MoS<sub>2</sub> supercell and the molecule, and  $E_{\text{Mol}}$  and  $E_{\text{MoS}_2}$  are the energies of the isolated molecule and MoS<sub>2</sub> rectangular supercell as defined previously, respectively. At first we consider pristine MoS<sub>2</sub> which is poorly reactive. In that respect, the molecular adsorption is driven by van der Waals interaction [53], and its inclusion in the calculations is of paramount importance. Unfortunately, this is not very convenient for designing electronic devices, as the molecules are very mobile in that configuration, with a high probability of diffusion with the temperature. For example, if we consider a CO<sub>2</sub> molecule on pristine MoS<sub>2</sub>, we obtain an equilibrium distance of 3.40 Å, for an adsorption energy of about -0.15 eV. This is in agreement with previous calculations on a large range of small molecules [54–56]. Consequently, we turn now to the study of molecular adsorption on the MoS<sub>2</sub> defects that we have considered in the previous sections. In Tables 2 and 3, we present respectively the adsorption energies and equilibrium distances determined in DFT+vdW for a series of small inorganic molecules adsorbed on different MoS<sub>2</sub> defects.

From these results, we can deduce a general trend which is that the most reactive defects for molecular adsorption are the metallic ones, namely the S mono- or divacancy with one or

**Table 2.** Adsorption energies (eV) at the most stable adsorption sites for each molecule

| Molecules | $E_{\text{Ads}}$ (eV) |       |                |                  |       |                |                |                 |
|-----------|-----------------------|-------|----------------|------------------|-------|----------------|----------------|-----------------|
|           | CO <sub>2</sub>       | CO    | O <sub>2</sub> | H <sub>2</sub> O | NO    | N <sub>2</sub> | H <sub>2</sub> | NO <sub>2</sub> |
| Pristine  | -0.15                 | -0.09 | -0.11          | -0.14            | -0.15 | -0.09          | -0.06          | -0.28           |
| vacS      | -0.16                 | -0.14 | -3.04          | -0.25            | -2.88 | -0.12          | -0.08          | -0.28           |
| vacS+Mo   | -0.59                 | -1.95 | -5.12          | -1.05            | -3.15 | -1.54          | -1.14          | -3.67           |
| vacMo     | -0.17                 | -0.11 | -2.49          | -0.16            | -0.22 | -0.10          | -0.06          | -1.05           |
| vacMo+S   | -0.14                 | -0.10 | -0.61          | -0.19            | -0.90 | -0.09          | -0.06          | -0.46           |
| vacMo+S2  | -0.14                 | -0.10 | -0.55          | -0.08            | -0.12 | -0.09          | -0.05          | -0.34           |
| vacS2     | -0.16                 | -0.14 | -3.11          | -0.24            | -2.93 | -0.11          | -0.08          | -0.25           |
| vacS2+Mo  | -0.41                 | -1.04 | -4.12          | -1.28            | -3.10 | -0.09          | -0.52          | -4.23           |
| vacS2+Mo2 | -1.19                 | -1.84 | -4.88          | -1.63            | -4.21 | -1.16          | -0.78          | -3.21           |

Reprinted from Ref. [46], copyright RSC 2017.

**Table 3.** Equilibrium distance (Å) at the most stable adsorption sites for each molecule

| Molecules | $\Delta h$ (Å)  |      |                |                  |      |                |                |                 |
|-----------|-----------------|------|----------------|------------------|------|----------------|----------------|-----------------|
|           | CO <sub>2</sub> | CO   | O <sub>2</sub> | H <sub>2</sub> O | NO   | N <sub>2</sub> | H <sub>2</sub> | NO <sub>2</sub> |
| Pristine  | 3.32            | 3.36 | 2.78           | 2.37             | 2.73 | 3.53           | 2.75           | 2.74            |
| vacS      | 2.97            | 2.09 | —*             | 0.85             | 1.01 | 2.90           | 1.90           | 2.16            |
| vacS+Mo   | 2.36            | 2.00 | 2.01           | 2.29             | 1.82 | 1.98           | —*             | —*              |
| vacMo     | 3.30            | 3.00 | —*             | 2.37             | 0.95 | 3.53           | 3.30           | 1.59            |
| vacMo+S   | 3.50            | 3.25 | 1.66           | 2.37             | 1.92 | 3.50           | 2.83           | 2.31            |
| vacMo+S2  | 3.51            | 1.92 | 2.52           | 2.70             | 2.51 | 3.00           | 3.23           | 2.72            |
| vacS2     | 2.95            | 2.30 | —*             | 1.05             | 1.13 | 3.04           | 2.60           | 2.85            |
| vacS2+Mo  | 2.31            | 2.20 | 2.01           | 2.21             | 1.82 | 2.10           | 1.89           | —*              |
| vacS2+Mo2 | 2.24            | 2.05 | 2.01           | 2.21             | 1.81 | 2.05           | 1.88           | —*              |

The sites labelled with \* correspond to the dissociative cases.

Reprinted from Ref. [46], copyright RSC 2017.

two Mo substitutions. In particular, we can observe that the CO<sub>2</sub> molecule remains physisorbed for all the S or Mo vacancies, and increases drastically its adsorption energy in contact with 2 Mo substitutions in a S divacancy, which is the most interacting adsorption site for almost all the molecules. This is due to the metallic states that close the electronic gap of MoS<sub>2</sub> or to the metallic states located very close to the Fermi level. In that respect, a strong bonding is established between the substituting Mo atom and its metallic states, and the inorganic molecule. Also, we have determined the charge transfer between these metallic defects and the molecules and have found that it is not very important, around 0.04 e, in particular for CO<sub>2</sub> or CO molecules. This means that these molecules are very stable upon adsorption on the MoS<sub>2</sub> layer, and that they can be imaged or characterized through STM or AFM. As explained in the previous section, this adsorption process on metallic defects is favored by a metal-semiconductor junction, which appears to be very important for the understanding of defects in TMDC. Also, we can stress the fact that homonuclear diatomic molecules like O<sub>2</sub>, N<sub>2</sub> and H<sub>2</sub> present slightly different behavior with for example higher charge transfers, around 0.25–0.35 e. Finally, we have considered dissociation processes on MoS<sub>2</sub> defects, as a probe for MoS<sub>2</sub> catalytic activity. We have found for example, that molecules containing oxygen (CO<sub>2</sub>, NO<sub>2</sub>, ...) present a certain ability to dissociate on S vacancies at room temperature. The O atoms have the same electronic

configuration as the S atoms, favouring their absorption in the S-vacancies. This obviously opens many promising perspectives for applications in gas storage or gas sensors.

Now that we have characterized the adsorption process of molecules on MoS<sub>2</sub> defects, we will consider the implications on conductance and force measurements.

### 3.2. *Conductances and forces on molecular adsorbed on defective MoS<sub>2</sub>*

Here we will consider the most reactive site for molecular adsorption on MoS<sub>2</sub>, as described earlier, which is the S divacancy with two Mo substitutions. As we have seen before, the small inorganic molecules are strongly bonded on this site, and therefore we can measure their conductance or forces by approaching a STM or AFM tip [57]. This method aims at developing a new way to detect molecules on very reactive sites. In Figure 5, we present the evolution of the calculated forces and electrical conductance, as a function of the tip-molecule distance, for the different molecules discussed previously, adsorbed on the two Mo substituting S divacancy.

The first important aspect that we can deduce from these results, is that the combination of conductance and force measurements for each molecule adsorbed on the reactive site, constitutes a clear signature of the molecule. Indeed, considering to discriminate these systems based on force or conductance curves only might result very complicated and confusing as some results are really close. However, the combination of both is much more powerful. For instance, considering the force curves presented in Figure 5(a), we can observe different intensities through the minimum of the curve, each at a specific tip-molecule distance. This represents one clear fingerprint of the system. The most important force is then obtained for the N<sub>2</sub> molecule, with around  $-1.50$  nN, at an apex distance of around  $3.1$  Å. Another clear fingerprint is extracted from conductance measurements, with the maximum conductance plateau and its value. For example, the highest conductance is obtained here for the H<sub>2</sub>O molecule, with  $1.1 G_0$ . Also the shape of the conductance is indicative, as some curves grow monotonically (H<sub>2</sub>O, CO<sub>2</sub>, ...) whereas others present a clear step of conductance before reaching the plateau (CO, NO, N<sub>2</sub>, ...). Also, homonuclear molecules present the same conductance (O<sub>2</sub>, N<sub>2</sub>) whereas heteronuclear ones present a different value (NO), which facilitates their discrimination. Obviously, as we have discussed before, the chemical nature of the tip will have an influence on the obtained results, either on the force measurements (example of reactive Cu tip versus non-reactive Si tip), or on the conductance measurements through the work function of the material. Therefore, one has to use the same tip to probe the different molecules through conductance and force measurements. Clearly, this is a hard task to keep the same tip for different measurements on different systems, however the measurements in a specific range of forces and conductance should be sufficient to provide a general trend in order to identify the adsorbed molecule fingerprint.

In the next and final result section, we will consider another way to characterize MoS<sub>2</sub> defects or adsorbed molecules on MoS<sub>2</sub> defects through the use of lateral junctions and lateral conductance measurements.

## 4. Lateral junctions: conductance calculations

In the previous sections, using DFT we have modelled several types of defect in MoS<sub>2</sub>, as well as molecules adsorbed on these defects. In that respect, we have simulated the corresponding STM images and we have determined the forces that we can compare to AFM experimental measurements. Also, we have determined the conductance, and together with the force, we have seen that it can be assigned to a specific adsorbed molecule, through its particular fingerprint. Hence, we have developed a method which together with experimental results, allows to characterize specific point defects on the MoS<sub>2</sub> monolayer, and to conceive nanodevices or gas sensors.

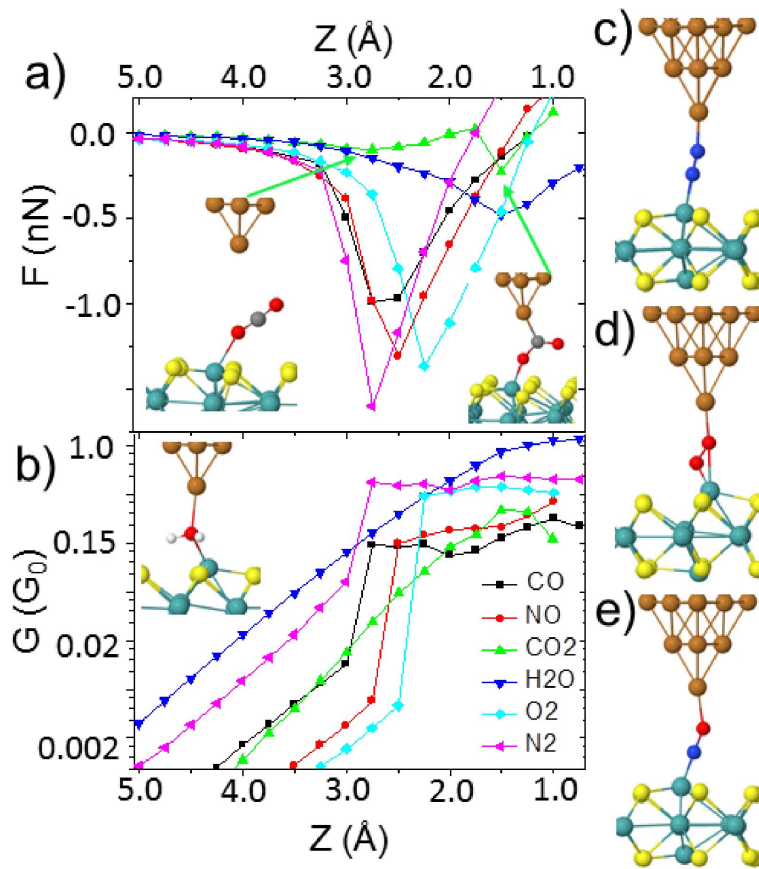


**Figure 5.** Calculated (a) forces and (b) conductance (in logarithmic scale) for different molecules adsorbed on the defective MoS<sub>2</sub> monolayer: CO (black squares), NO (red circles), CO<sub>2</sub> (green uptriangles), H<sub>2</sub>O (blue down-triangles), O<sub>2</sub> (light-blue rhombus), and N<sub>2</sub> (pink left-triangles). Lateral view of the contact formed between the Cu tip (brown spheres) and the different molecules: (c) N<sub>2</sub>, (d) O<sub>2</sub>, and (e) NO molecules. Inset: The atomic configuration corresponding to both minima of the force in the CO<sub>2</sub> case and the H<sub>2</sub>O molecule. The light-blue, yellow, dark-blue, red, and white spheres correspond to Mo, S, N, O, and H, respectively. Reprinted with permission from Ref. [57], copyright APS 2016.

In this last section, we present new results where we consider defective MoS<sub>2</sub> nanoribbons, sandwiched between two gold electrodes. Hence, we now consider lateral junctions of defective MoS<sub>2</sub>, meaning that the MoS<sub>2</sub> nanoribbon is connected in the plane, on two sides of the nanoribbon, and not perpendicularly as in the case of STM or AFM experiments. This geometry is a bit different from the one we considered before when we have probed point defects using STM or AFM. The present geometry resembles what is used in nanoelectronic devices. In this case, we do not probe anymore the conductance between the tip and a defective 2D material, but we fully probe the electronic transport in the plane of the bidimensional material. It is therefore very interesting on a fundamental point of view. Also, in order to design gas sensors for example, this geometry is more adapted, since we do not need a STM or AFM apparatus to characterize the defect. A simple current measurement should give us access to the modification of the sensor in case of adsorbed



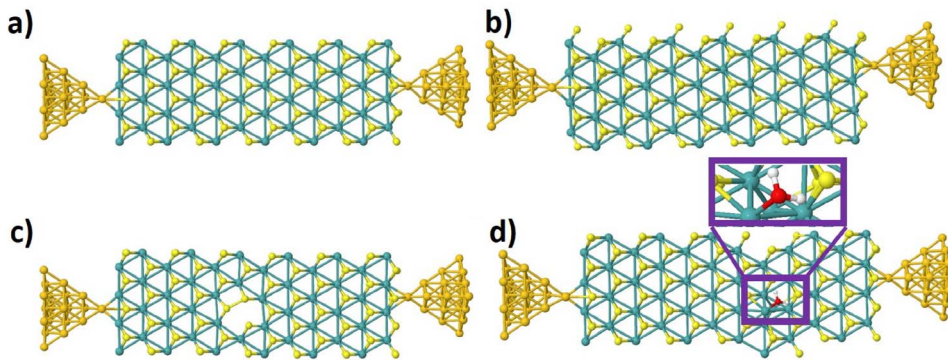


**Figure 6.** Some optimized configurations for defective MoS<sub>2</sub> nanoribbons sandwiched between gold electrodes: (a) clean MoS<sub>2</sub>, (b) S vacancy, (c) Mo vacancy and (d) S divacancy with two Mo substitutional atoms, and an adsorbed water molecule, with an inset focusing on the molecule. The gold, light-blue, yellow, red, and white spheres correspond to Au, Mo, S, O, and H, respectively.

gas. Some examples of these lateral junctions unit cells are presented in Figure 6.

We have considered here the same defects as those previously studied, and enlarged the unit cell in the electrode direction to avoid direct electrode coupling. The direction perpendicular to the electrode remains periodic. Hence, we have in Figure 6(a) the clean MoS<sub>2</sub>, (b) the S vacancy, (c) the Mo vacancy and (d) the S divacancy plus two Mo substitutional atoms and a water molecule. Each unit cell has been optimized using Fireball, and the electronic transport has been determined using the same formalism previously used for STM image calculations, one electrode being the tip and the other one plus the defective nanoribbon being the sample in the formalism.

As a result, we represent in Figure 7 the evolution of the electrical conductance for each defect configuration.

At first, we can observe that generally speaking, the calculated lateral conductances are much higher than their vertical counterpart when we were calculating the local conductance for the system in interaction with a STM tip. For example, the conductance of the defect formed by two Mo atoms in a S divacancy in MoS<sub>2</sub> with a O<sub>2</sub>, CO, or NO molecule adsorbed on top lies around 0.37–0.44 G<sub>0</sub>, whereas they were about 0.13–0.18 G<sub>0</sub> when probed by a STM tip. The only exception is the water molecule on the Mo substitution on the S divacancy defect in MoS<sub>2</sub>, which presents a conductance of 0.3 G<sub>0</sub>, whereas it reaches almost 1.0 G<sub>0</sub> when probed by a STM Cu tip. On another hand, the defect presenting the highest conductance, and with the biggest difference with respect to clean MoS<sub>2</sub> (about 0.52 G<sub>0</sub>), is the Mo vacancy with a conductance of almost 0.7 G<sub>0</sub>. This might be exploited for nanoelectronic devices, since the electronic response is increased by about 40%. Surprisingly, a S vacancy saturated with Mo substituent or a S divacancy saturated by two Mo substituents present very similar electrical responses, with a conductance around 0.42 G<sub>0</sub>. In that respect, the adsorption of small molecules on these defects does not affect really the overall conductance, except for NO<sub>2</sub>, which helps reaching the conductance of clean MoS<sub>2</sub>, and NO, H<sub>2</sub> and H<sub>2</sub>O which lower the conductance until 0.35 G<sub>0</sub>. Again, a water molecule on two Mo in a S divacancy defect yields the lowest conductance. All in all, two Mo atoms in a S divacancy constitutes a rather promising gas sensor for NO<sub>2</sub>, NO, H<sub>2</sub>O and H<sub>2</sub>. Obviously, additional cases should be tested with different molecules on different defects, like the evolution of the Mo vacancy upon molecular adsorption for example, but our aim here is only to present the proof of concept of a potential method for gas sensing.

The conductance difference between vertical and lateral conductance is probably due to the



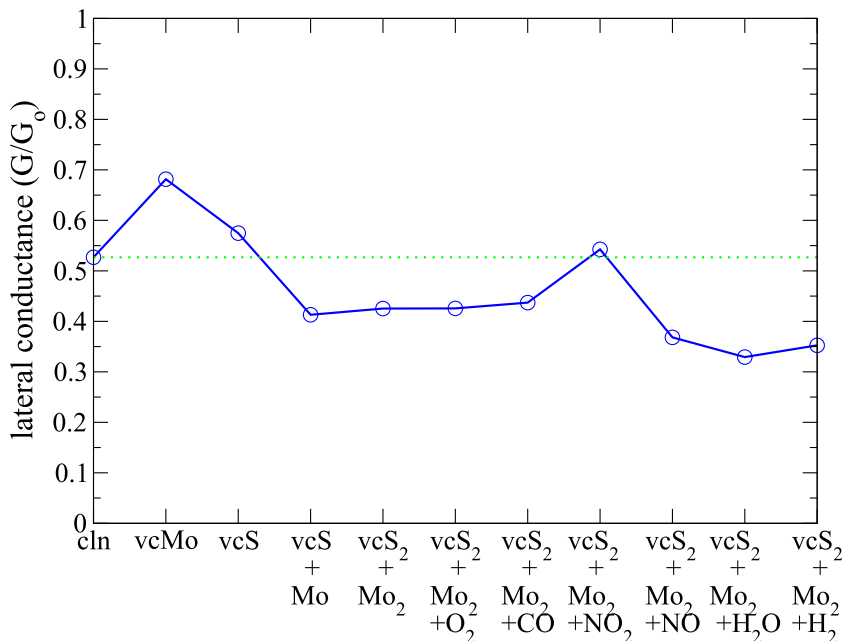


**Figure 7.** Evolution of the lateral conductance calculated for different defective MoS<sub>2</sub> nanoribbons: clean, Mo and S vacancy, S vacancy + Mo, S divacancy + Mo<sub>2</sub>, S divacancy + Mo<sub>2</sub> + O<sub>2</sub> or CO or NO<sub>2</sub> or NO or H<sub>2</sub>O or H<sub>2</sub>. The dashed green line represents the conductance value of the clean MoS<sub>2</sub> nanoribbon, to facilitate the comparison for the other structures.

bottleneck of the electric current at the interface between the tip and the molecule. Obviously the transport mechanism is rather different here, since we are probing electronic states in the gap of the MoS<sub>2</sub>, and we consider the propagation of the current all along the nanoribbon. Intuitively, we can consider that the introduction of metallic states in the gap (as it is obtained by the substitution of the two Mo atoms in the S divacancy) will favor the electronic transport in the MoS<sub>2</sub> nanoribbon. Also, we have to take into account the fact that the limits of the nanoribbon connected to the gold electrodes will create new states in the MoS<sub>2</sub> gap and affect the global electronic structure. In that respect, we present in Figure 8 the electronic transmission for different defects considered here.

As we can observe, the electronic structure of MoS<sub>2</sub> is greatly affected by the nanoribbon shape, introducing a strong localized state at the Fermi level for all the defective nanoribbons. These results show that there is no more gap in these MoS<sub>2</sub> nanoribbons, so the effect of the edges is still important for this size. Hence, the variation of conductance presented in Figure 7 is related to the localization of this peak in the vicinity of the Fermi level. Indeed, for clean MoS<sub>2</sub>, the peak is located just below the Fermi level, as for the common S vacancy, which explains the very similar conductance. Also, this means that the S vacancy does not affect drastically the electronic transport in the MoS<sub>2</sub> nanoribbon. On the other side, the Mo vacancy presents a peak slightly shifted toward the positive energies. This is easily understandable as the removal of a metallic atom induces a slight p doping in the system. In that respect the conductance is much higher at the Fermi level due to the crossing of the peak. However, taking a look at the  $T(E)$  curves, we can infer that probably the inclusion of a voltage would increase the difference between the different defects.

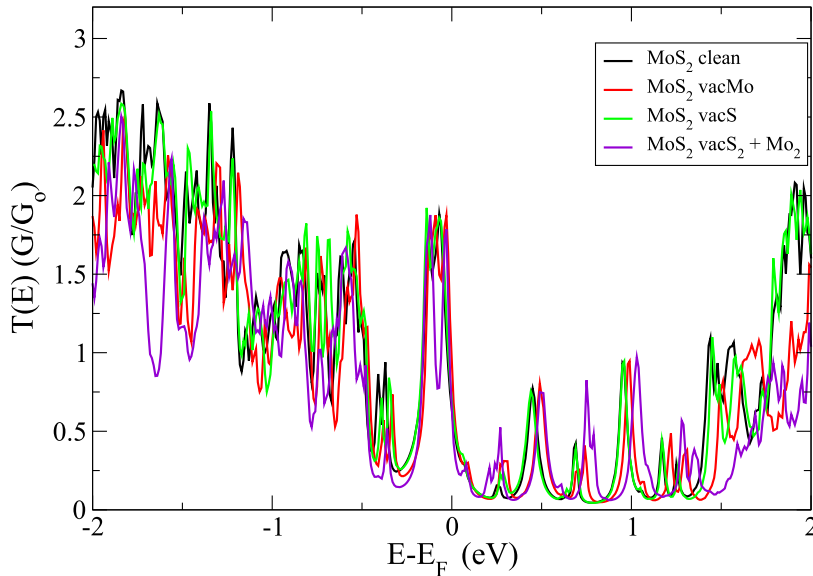


**Figure 8.** Evolution of the electronic transmissions calculated for the different defective MoS<sub>2</sub> nanoribbons presented in Figure 7.

## 5. Conclusions and perspectives

To summarize, we have presented here a mini-review on our exhaustive work on defects in a MoS<sub>2</sub> monolayer. Using DFT calculations, we have defined and characterized these defects, mainly based on Mo and S vacancies, and their substitutional atoms. In particular we have determined their structure and formation energies, and shown the modulation of the local electronic properties through electronic gap reduction or emergence of very reactive metallic states in the gap. Then, we have modelled the corresponding STM images, in order to establish comparison with experiments and to interpret future experimental results. We have shown in particular how a nitrogen substitution in a S vacancy has been identified in a recent STM experiment using our method. Also, we have calculated the forces between the different defects and an AFM tip, as a complementary tool to identify their respective fingerprint.

Once this methodology has been established, we have considered the adsorption of small inorganic molecules on defective MoS<sub>2</sub>, as a probe for the induced local reactivity. Also, we have calculated conductance and forces between a metallic tip and the adsorbed molecules. As a result, we show that the combination of both calculations (and accordingly measurements, on the experimental side), constitute an accurate way of characterizing these molecules on the defects.

Finally, we have presented very recent results on lateral defective MoS<sub>2</sub> nanoribbons sandwiched between gold electrodes. In these nanojunctions, we consider the same defects as studied previously, and we compare their lateral conductance with what has been obtained previously in STM configuration. We also reveal the most interesting defects for applications, accordingly to their electrical response through the calculation and analysis of the electronic transmission.

This work obviously presents many perspectives. At first, we have established here a simple and complete methodology for characterizing point defects and adsorbed molecules on MoS<sub>2</sub>, as a full support for experimental measurements. Second, the observed modifications of their electronic structure make these materials very promising for applications in nanoelectronics. Indeed, a wide variety of new devices can be designed exploiting the new metallic states emerging in the electronic gap. Also, these new states appear to be very reactive and can be exploited for

catalysis, or to favor molecular adsorption. In that respect, defective MoS<sub>2</sub>, or as presented in the last section defective MoS<sub>2</sub> nanoribbons offer interesting perspectives for gas sensors, since molecular adsorption modifies the electrical response of the system.

Finally, the last section presented here illustrates also the need to achieve further analysis on the response of the defective MoS<sub>2</sub> nanoribbons. Indeed, the size of the ribbon and its incidence on the electronic properties have to be further explored, in order to limit at most the edge effects. Also, the possibility of gating the nanoribbons has to be considered as well, as the application of a voltage might help in discriminating the different defects (or modifying their reactivity) in order to refine their fingerprint. Last but not least, this study can be generalized to other kinds of defects like grain boundaries for example.

## Acknowledgements

The first author acknowledges financial support from the Community of Madrid through the project NANOMAGCOST, ref P2018/NMT-4321. Also, the authors thankfully acknowledge the computer resources at Calendula and technical support provided by Scayle (projects FI-2020-2-0022 and FI-2020-3-0033).

## References

- [1] K. S. Novoselov, A. K. Geim, S. V. Morozov, D. Jiang, Y. Zhang, S. V. Dubonos, I. V. Grigorieva, A. A. Firsov, "Electric field effect in atomically thin carbon films", *Science* **306** (2004), no. 5696, p. 666-669.
- [2] E. N. Voloshina, Y. S. Dedkov, S. Torbrügge, A. Thissen, M. Fonin, "Graphene on Rh(111): scanning tunneling and atomic force microscopy studies", *Appl. Phys. Lett.* **100** (2012), no. 24, article no. 241606.
- [3] K. Xu, P. Cao, J. R. Heath, "Scanning tunneling microscopy characterization of the electrical properties of wrinkles in exfoliated graphene monolayers", *Nano Lett.* **9** (2009), no. 12, p. 4446-4451.
- [4] A. H. Castro Neto, F. Guinea, N. M. R. Peres, K. S. Novoselov, A. K. Geim, "The electronic properties of graphene", *Rev. Mod. Phys.* **81** (2009), p. 109-162.
- [5] X. Han, J. Lin, J. Liu, N. Wang, D. Pan, "Effects of hexagonal boron nitride encapsulation on the electronic structure of few-layer MoS<sub>2</sub>", *J. Phys. Chem. C* **123** (2019), no. 23, p. 14797-14802.
- [6] S. Liu, K. Yuan, X. Xu, R. Yin, D.-Y. Lin, Y. Li, K. Watanabe, T. Taniguchi, Y. Meng, L. Dai, Y. Ye, "Hysteresis-free hexagonal boron nitride encapsulated 2D semiconductor transistors, NMOS and CMOS inverters", *Adv. Electron. Mater.* **5** (2019), no. 2, article no. 1800419.
- [7] S. Manzeli, D. Ovchinnikov, D. Pasquier, O. V. Yazyev, A. Kis, "2D transition metal dichalcogenides", *Nat. Rev. Mater.* **2** (2017), article no. 17033.
- [8] H. S. Nalwa, "A review of molybdenum disulfide (MoS<sub>2</sub>) based photodetectors: from ultra-broadband, self-powered to flexible devices", *RSC Adv.* **10** (2020), p. 30529-30602.
- [9] F. Giannazzo, E. Schilirò, G. Greco, F. Roccaforte, "Conductive atomic force microscopy of semiconducting transition metal dichalcogenides and heterostructures", *Nanomaterials* **10** (2020), no. 4, article no. 803.
- [10] X. Li, H. Zhu, "Two-dimensional MoS<sub>2</sub>: properties, preparation, and applications", *J. Materiomics* **1** (2015), no. 1, p. 33-44.
- [11] D. R. Klein, D. MacNeill, J. L. Lado, D. Soriano, E. Navarro-Moratalla, K. Watanabe, T. Taniguchi, S. Manni, P. Canfield, J. Fernández-Rossier, P. Jarillo-Herrero, "Probing magnetism in 2D van der Waals crystalline insulators via electron tunneling", *Science* **360** (2018), no. 6394, p. 1218-1222.
- [12] X. Zhang, D. Sun, Y. Li, G.-H. Lee, X. Cui, D. Chenet, Y. You, T. F. Heinz, J. C. Hone, "Measurement of lateral and interfacial thermal conductivity of single- and bilayer MoS<sub>2</sub> and MoSe<sub>2</sub> using refined optothermal Raman technique", *ACS Appl. Mater. Interfaces* **7** (2015), no. 46, p. 25923-25929.
- [13] W. Zhang, J.-Y. Yang, L. Liu, "Strong interfacial interactions induced a large reduction in lateral thermal conductivity of transition-metal dichalcogenide superlattices", *RSC Adv.* **9** (2019), p. 1387-1393.
- [14] A. K. Geim, I. V. Grigorieva, "Van der waals heterostructures", *Nature* **499** (2013), no. 7459, p. 419-425.
- [15] W. Liao, Y. Huang, H. Wang, H. Zhang, "Van der Waals heterostructures for optoelectronics: progress and prospects", *Appl. Mater. Today* **16** (2019), p. 435-455.
- [16] C. Li, P. Zhou, D. W. Zhang, "Devices and applications of van der Waals heterostructures", *J. Semicond.* **38** (2017), no. 3, article no. 031005.

- [17] R. Xiang, T. Inoue, Y. Zheng, A. Kumamoto, Y. Qian, Y. Sato, M. Liu, D. Tang, D. Gokhale, J. Guo, K. Hisama *et al.*, “One-dimensional van der waals heterostructures”, *Science* **367** (2020), no. 6477, p. 537-542.
- [18] J.-Y. Noh, H. Kim, Y.-S. Kim, “Stability and electronic structures of native defects in single-layer MoS<sub>2</sub>”, *Phys. Rev. B* **89** (2014), article no. 205417.
- [19] W. Zhou, X. Zou, S. Najmaei, Z. Liu, Y. Shi, J. Kong, J. Lou, P. M. Ajayan, B. I. Yakobson, J.-C. Idrobo, “Intrinsic structural defects in monolayer molybdenum disulfide”, *Nano Lett.* **13** (2013), no. 6, p. 2615-2622.
- [20] J. Hong, Z. Hu, M. Probert, K. Li, D. Lv, X. Yang, L. Gu, N. Mao, Q. Feng, L. Xie *et al.*, “Exploring atomic defects in molybdenum disulphide monolayers”, *Nat. Commun.* **6** (2015), no. 1, article no. 6293.
- [21] B. Mondal, A. Som, I. Chakraborty, A. Bakshi, D. Sarkar, T. Pradeep, “Unusual reactivity of MoS<sub>2</sub> nanosheets”, *Nanoscale* **8** (2016), p. 10282-10290.
- [22] X. Chen, S. M. Shinde, K. P. Dhakal, S. W. Lee, H. Kim, Z. Lee, J.-H. Ahn, “Degradation behaviors and mechanisms of MoS<sub>2</sub> crystals relevant to bioabsorbable electronics”, *NPG Asia Mater.* **10** (2018), no. 8, p. 810-820.
- [23] M. Mohan, V. K. Singh, S. Reshmi, S. R. Barman, K. Bhattacharjee, “Atomic adsorption of Sn on mechanically cleaved WS<sub>2</sub> surface at room temperature”, *Surf. Sci.* **701** (2020), article no. 121685.
- [24] S. G. Sorensen, H. G. Füchtbauer, A. K. Tuxen, A. S. Walton, J. V. Lauritsen, “Structure and electronic properties of in situ synthesized single-layer MoS<sub>2</sub> on a gold surface”, *ACS Nano* **8** (2014), no. 7, p. 6788-6796.
- [25] K. C. Santosh, R. C. Longo, R. Addou, R. M. Wallace, K. Cho, “Impact of intrinsic atomic defects on the electronic structure of MoS<sub>2</sub> monolayers”, *Nanotechnology* **25** (2014), no. 37, article no. 375703.
- [26] N. Kodama, T. Hasegawa, Y. Okawa, T. Tsuruoka, C. Joachim, M. Aono, “Electronic states of sulfur vacancies formed on a MoS<sub>2</sub> surface”, *Japanese J. Appl. Phys.* **49** (2010), no. 8, article no. 08LB01.
- [27] M. Makarova, Y. Okawa, M. Aono, “Selective adsorption of thiol molecules at sulfur vacancies on MoS<sub>2</sub> (0001), followed by vacancy repair via S<sub>2</sub> dissociation”, *J. Phys. Chem. C* **116** (2012), no. 42, p. 22411-22416.
- [28] H.-P. Komsa, A. V. Krasheninnikov, “Native defects in bulk and monolayer MoS<sub>2</sub> from first principles”, *Phys. Rev. B* **91** (2015), article no. 125304.
- [29] R. Thamankar, T. L. Yap, K. E. J. Goh, C. Troadec, C. Joachim, “Low temperature nanoscale electronic transport on the MoS<sub>2</sub> surface”, *Appl. Phys. Lett.* **103** (2013), no. 8, article no. 083106.
- [30] S. Zhao, J. Xue, W. Kang, “Gas adsorption on MoS<sub>2</sub> monolayer from first-principles calculations”, *Chem. Phys. Lett.* **595-596** (2014), p. 35-42.
- [31] G. Froehlicher, E. Lorchat, S. Berciaud, “Direct versus indirect band gap emission and exciton-exciton annihilation in atomically thin molybdenum ditelluride (MoTe<sub>2</sub>)”, *Phys. Rev. B* **94** (2016), article no. 085429.
- [32] C. González, B. Biel, Y. J. Dappe, “Theoretical characterisation of point defects on a MoS<sub>2</sub> monolayer by scanning tunnelling microscopy”, *Nanotechnology* **27** (2016), no. 10, article no. 105702.
- [33] J. P. Lewis, P. Jelínek, J. Ortega, A. A. Demkov, D. G. Trabada, B. Haycock, H. Wang *et al.*, “Advances and applications in the FIREBALL ab initio tight-binding molecular-dynamics formalism”, *Phys. Status Solidi (b)* **248** (2011), no. 9, p. 1989-2007.
- [34] P. Jelínek, H. Wang, J. P. Lewis, O. F. Sankey, J. Ortega, “Multicenter approach to the exchange-correlation interactions in ab initio tight-binding methods”, *Phys. Rev. B* **71** (2005), article no. 235101.
- [35] O. F. Sankey, D. J. Niklewski, “Ab initio multicenter tight-binding model for molecular-dynamics simulations and other applications in covalent systems”, *Phys. Rev. B* **40** (1989), p. 3979-3995.
- [36] J. Harris, “Simplified method for calculating the energy of weakly interacting fragments”, *Phys. Rev. B* **31** (1985), p. 1770-1779.
- [37] W. M. C. Foulkes, R. Haydock, “Tight-binding models and density-functional theory”, *Phys. Rev. B* **39** (1989), p. 12520-12536.
- [38] M. A. Basanta, Y. J. Dappe, P. Jelínek, J. Ortega, “Optimized atomic-like orbitals for first-principles tight-binding molecular dynamics”, *Comput. Mater. Sci.* **39** (2007), no. 4, p. 759-766.
- [39] C. González, E. Abad, Y. J. Dappe, J. C. Cuevas, “Theoretical study of carbon-based tips for scanning tunnelling microscopy”, *Nanotechnology* **27** (2016), no. 10, article no. 105201.
- [40] I. Horcas, R. Fernández, J. M. Gómez-Rodríguez, J. Colchero, J. Gómez-Herrero, A. M. Baro, “WSXM: A software for scanning probe microscopy and a tool for nanotechnology”, *Rev. Sci. Instrum.* **78** (2007), no. 1, article no. 013705.
- [41] C. González, D. Fernández-Pello, M. A. Cerdeira, S. L. Palacios, R. Iglesias, “Helium bubble clustering in copper from first principles”, *Model. Simul. Mater. Sci. Eng.* **22** (2014), no. 3, article no. 035019.
- [42] G. Kresse, J. Hafner, “Ab initio molecular dynamics for liquid metals”, *Phys. Rev. B* **47** (1993), p. 558-561.
- [43] G. Kresse, J. Furthmüller, “Efficient iterative schemes for ab initio total-energy calculations using a plane-wave basis set”, *Phys. Rev. B* **54** (1996), p. 11169-11186.
- [44] G. Kresse, D. Joubert, “From ultrasoft pseudopotentials to the projector augmented-wave method”, *Phys. Rev. B* **59** (1999), p. 1758-1775.
- [45] C. González, Y. J. Dappe, B. Biel, “Reactivity enhancement and fingerprints of point defects on a MoS<sub>2</sub> monolayer assessed by ab initio atomic force microscopy”, *J. Phys. Chem. C* **120** (2016), no. 30, p. 17115-17126.

- [46] C. González, B. Biel, Y. J. Dappe, “Adsorption of small inorganic molecules on a defective MoS<sub>2</sub> monolayer”, *Phys. Chem. Chem. Phys.* **19** (2017), p. 9485-9499.
- [47] S. Dubey, S. Lisi, G. Nayak, F. Herziger, V.-D. Nguyen, T. Le Quang, V. Cherkez, C. González, Y. J. Dappe, K. Watanabe, T. Taniguchi *et al.*, “Weakly trapped, charged, and free excitons in single-layer MoS<sub>2</sub> in the presence of defects, strain, and charged impurities”, *ACS Nano* **11** (2017), no. 11, p. 11206-11216.
- [48] S. Barja, S. Wickenburg, Z.-F. Liu, Y. Zhang, H. Ryu, M. M. Ugeda, Z. Hussain, Z.-X. Shen *et al.*, “Charge density wave order in 1D mirror twin boundaries of single-layer MoSe<sub>2</sub>”, *Nature Phys.* **12** (2016), no. 8, p. 751-756.
- [49] X. Liu, Z. G. Yu, G. Zhang, Y.-W. Zhang, “Remarkably high thermal-driven MoS<sub>2</sub> grain boundary migration mobility and its implications on defect healing”, *Nanoscale* **12** (2020), p. 17746-17753.
- [50] M. Ondráček, P. Pou, V. Rozsival, C. González, P. Jelínek, R. Pérez, “Forces and currents in carbon nanostructures: are we imaging atoms?”, *Phys. Rev. Lett.* **106** (2011), article no. 176101.
- [51] O. Custance, R. Perez, S. Morita, “Atomic force microscopy as a tool for atom manipulation”, *Nat. Nanotechnol.* **4** (2009), no. 12, p. 803-810.
- [52] Y. Sugimoto, P. Pou, O. Custance, P. Jelinek, M. Abe, R. Perez, S. Morita, “Complex patterning by vertical interchange atom manipulation using atomic force microscopy”, *Science* **322** (2008), no. 5900, p. 413-417.
- [53] U. Patil, N. M. Caffrey, “Adsorption of common solvent molecules on graphene and MoS<sub>2</sub> from first-principles”, *J. Chem. Phys.* **149** (2018), no. 9, article no. 094702.
- [54] Q. H. Wang, K. Kalantar-Zadeh, A. Kis, J. N. Coleman, M. S. Strano, “Electronics and optoelectronics of two-dimensional transition metal dichalcogenides”, *Nat. Nanotechnol.* **7** (2012), no. 11, p. 699-712.
- [55] N. Myoung, K. Seo, S. J. Lee, G. Ihm, “Large current modulation and spin-dependent tunneling of vertical graphene/MoS<sub>2</sub> heterostructures”, *ACS Nano* **7** (2013), no. 8, p. 7021-7027.
- [56] N. Aguilar, S. Aparicio, “Theoretical insights into CO<sub>2</sub> adsorption by MoS<sub>2</sub> nanomaterials”, *J. Phys. Chem. C* **123** (2019), no. 43, p. 26338-26350.
- [57] C. González, Y. J. Dappe, “Molecular detection on a defective MoS<sub>2</sub> monolayer by simultaneous conductance and force simulations”, *Phys. Rev. B* **95** (2017), article no. 214105.